Bond and part strength in fused deposition modeling

Timothy J. Coogan
Saint-Gobain Northborough R&D Center, Northborough, Massachusetts, USA and
Department of Plastics Engineering, University of Massachusetts Lowell,
Lowell, Massachusetts, USA, and
David Owen Kazmer
Department of Plastics Engineering, University of Massachusetts Lowell, Lowell, Massachusetts, USA

Abstract

Purpose – The purpose of this paper is to investigate the factors governing bond strength in fused deposition modeling (FDM) compared to strength in the fiber direction.

Design/methodology/approach – Acrylonitrile butadiene styrene (ABS) boxes with the thickness of a single fiber were made at different platform and nozzle temperatures, print speeds, fiber widths and layer heights to produce multiple specimens for measuring the strength.

Findings – Specimens produced with the fibers oriented in the tensile direction had 95 per cent of the strength of the constitutive filament. Bond strengths ranged from 40 to 85 per cent of the filament strength dependent on the FDM processing conditions. Diffusion, wetting and intimate contact all separately affect bond strength.

Practical implications – This study provides processing recommendations for producing the strongest FDM parts. The needs for higher nozzle temperatures and more robust feed motors are described; these recommendations can be useful for companies producing FDM products as well as companies designing FDM printers.

Originality/value – This is the first study that discusses wetting and intimate contact separately in FDM, and the results suggest that a fundamental, non-empirical model for predicting FDM bond strength can be developed based on healing models. Additionally, the role of equilibration time at the start of extrusion as well as a motor torque limitation while trying to print at high speeds are described.

Keywords Solid freeform fabrication, Tensile strength, Thermoplastic polymers, Bond strength, Fused deposition modelling, Thermal diffusion

Paper type Research paper

Introduction

Fused deposition modeling (FDM) is a form of rapid prototyping where fibers are extruded so they lay adjacent to one another in the same layer, and then the layers are stacked upon one another to form a desired design. A typical FDM process as well as a depiction of defined terminology is shown in Figure 1. The starting material is a polymeric filament, which is fed into the 3D printer using drive wheels. The filament is forced through a heating element, also known as the liquefier, where the filament becomes molten prior to flowing out of the heated FDM nozzle at a controlled rate. The extruded filament is then referred to as a fiber. The moving nozzle deposits fibers onto a build platform that may be directly heated or otherwise reside in a temperature-controlled environment. The nozzle moves and prints at a controlled velocity, referred to as the print speed.

As shown in Figure 1, the nozzle is moving to the right to print a continuous fiber; this print direction is termed the longitudinal direction, and if the strength of the part was to be tested in the longitudinal direction, it would be referred to as the longitudinal strength. Alternatively, the strength perpendicular to the longitudinal direction reflects the adhesion between fibers, and is referred to as bond strength. When a fiber is being deposited, it has a given height and width as shown in Figure 1.

FDM not only produces parts for use as prototypes, models and molds but also is increasingly used as a production technique for commercial products such as medical implants (Espalin *et al.*, 2010). One of the biggest challenges in engineering FDM parts for end-use applications is predicting and assuring the mechanical properties of the FDM-made part (Garg *et al.*, 2014). Compared to conventional plastic processing techniques such as injection molding, FDM-made parts typically have lower mechanical properties because of the discontinuous nature of the process: adjacent fibers initially come into contact with one another while they are molten, but their rapid cooling process causes them to solidify prior to completely fusing with the other fibers, leaving voids between the fibers and interfaces that do not have full mechanical properties. In prior investigations, Ahn *et al.* (2002) studied the tensile strength of acrylonitrile butadiene styrene (ABS) produced through FDM. The longitudinal strength was 73 per cent of an injection molded part, which was attributed to

The current issue and full text archive of this journal is available on Emerald Insight at: **www.emeraldinsight.com/1355-2546.htm**

Rapid Prototyping Journal
23/2 (2017) 414–422

[DOI 10.1108/RPJ-03-2016-0050]

Received 31 March 2016
Revised 21 May 2016
Accepted 1 June 2016

Figure 1 Typical FDM process (left) and measured bond width and fiber width (right)

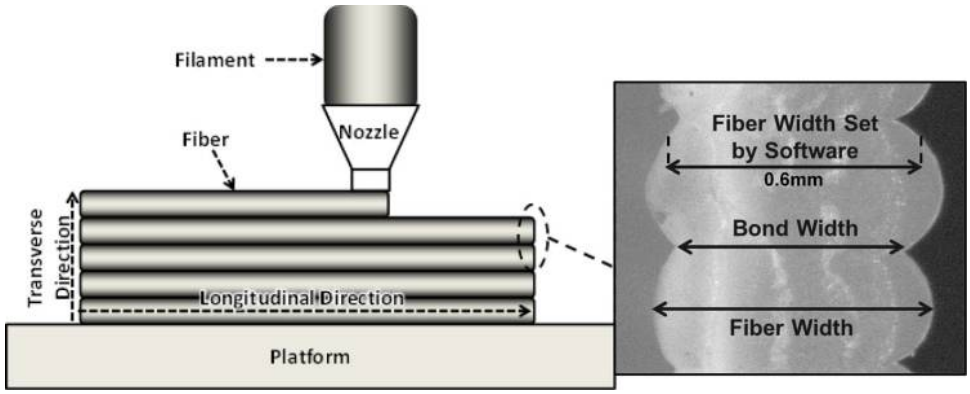

the decrease in cross-sectional area because of the voids between adjacent fibers. Moreover, the bond strength varied between 10 and 50 per cent of an injection molded part. A number of other studies found similar anisotropic results which were attributed to the weak interlayer bonds (Bellini and Güçeri, 2003; Li *et al.*, 2002a, 2001, 2002b; Bellehumeur *et al.*, 2004; Sun *et al.*, 2008; Thomas and Rodriguez, 2000; Rodríguez-Matas, 1999). Hill and Haghi (2014) recently investigated the direction dependence of FDM parts, finding that inter-fiber bonds were the weakest locations, but they did not analyze the underlying causality. The bond strength is a function of the interlayer wetting and polymer-chain diffusion (Turner *et al.*, 2014; Bellehumeur *et al.*, 2004; Sun *et al.*, 2008). Empirical models have been developed for predicting FDM outputs such as strength and surface roughness, but no theoretical models have been able to predict all the complexities of the FDM process (Garg *et al.*, 2014).

The authors now hypothesize that FDM bond strength can be described using a healing model similar to that proposed by Wool and O'Connor (1981, 1982). The healing across an interface can be viewed as taking place in five steps: surface rearrangement, surface approach, wetting, diffusion and randomization. Strength is dominated by wetting and diffusion, both of which occur more rapidly at higher temperatures and can continue to occur as long as the temperature is above the glass transition temperature, T_g. Therefore, the mechanical properties of an interface heal more quickly at higher temperatures (Wool and O'Connor, 1981, 1982). A transient heat model has been applied to the results presented in this paper, showing that temperature and diffusion affect the bond strength.

Method

Materials and equipment

All the parts were printed with filaments made of Cycolac MG47 ABS, supplied by SABIC, with a T_g of 113°C. The filament was extruded on a TMC-1 extruder with a 19 mm general purpose screw. The extruder was operated at 100 rpm with the barrel temperature set to 220°C. The die diameter was 1.9 mm with a pull speed of 5 m/min to create a filament with a diameter of 1.75 mm. Prior to extrusion, the ABS was dried at 80°C for 2 h.

An Ideator 12 printer from inDimension3 was used to print the parts. The printer does not have a controlled environmental chamber, but the platform can be controlled up to temperatures of 170°C. The length of the heating element plus the nozzle was 20 mm. Prior to use in FDM, the filament was dried for 4 h and pulled directly from an oven at 90°C so that it was completely dry, because filament moisture has been found to create defects during FDM (Turner *et al.*, 2014).

FDM printing conditions

Hollow boxes were printed using Simplify 3D (Cincinnati, OH) pre-processor. The boxes had 50.8 mm long walls with a 25.4 mm height as shown in Figure 2. Each layer started at wall "A" and finished at wall "D". The thickness of each wall was a single fiber width to facilitate dimensional analysis of the fiber width and bond width, as shown by a dimensional analysis example on the right side of Figure 1.

The following parameters were varied individually to determine their effect on tensile strength: platform temperature, nozzle temperature, print speed, fiber width and layer height. Low, medium and high values were chosen for each condition with the implemented design of experiments provided in Table I. The reference condition was chosen as the point where all the conditions were at their medium

Figure 2 FDM part (top) and tensile specimens cut from the part (bottom)

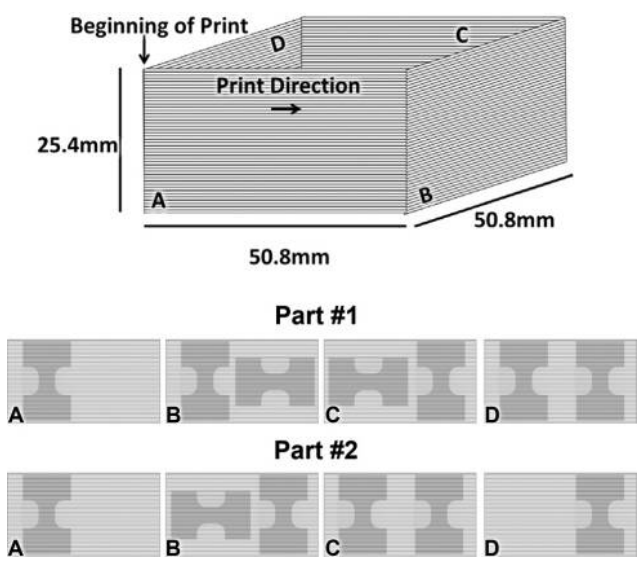

values. While varying one condition through its low, medium and high values, all the other conditions were set at their medium values. Boxes were successfully printed at all the run conditions. Two boxes were produced for each of the 11 conditions; however, additional boxes were made at the reference condition to provide replicates spaced throughout the entire set of experiments to determine if there was any effect from time, process order or changes in ABS filament. No effects from run order or time were observed, though variances in the filament were found to propagate as subsequently discussed.

Tensile specimen preparation

The tensile specimens were cut from the walls as shown in the bottom image of Figure 2, keeping track of their wall location (A to D) and orientation (top/bottom and inside/outside). The ten vertical specimens in Figure 2 were cut to test the bond strength between layers, and the three horizontal specimens were cut to test the longitudinal strength. The dimensions of the specimens, shown in Figure 3, were modified from the test specimen defined in ASTM D1708. The tensile parts were cut from the walls using a 40W Epilog Mini Laser cutter. A die cutter was also used to cut specimens from the blank locations in Figure 2. The die cut specimens were used for image analysis, such as the images shown in Figures 1 and 10, because the edges of the specimens cut with the laser cutter had melted. The bond strengths of six reference specimens cut with the die cutter were compared to the bond strengths of the specimens cut with the laser cutter, and the strengths from both methods were found to be statistically indistinguishable.

Tensile testing

The tensile testing was performed on an Instron 33R 4465 with Bluehill 3 software. The test was based on ASTM D1708, with accommodations for the small sample dimensions. A gauge length of 10 mm with a testing speed of 0.5 mm/min was used. The thickness of the parts for stress calculations was based on the specimen cross-section derived from the measured fiber width as shown in Figure 1. The tensile specimens shown in Figure 3 were clamped between rubber jaws at 75 psi. The strength of the initial ABS filament was also measured. Serrated metal clamps, with a tooth pitch of 1.4 mm and tooth angle of 120°, were needed for testing the

Figure 3 Dimensions of tensile specimens

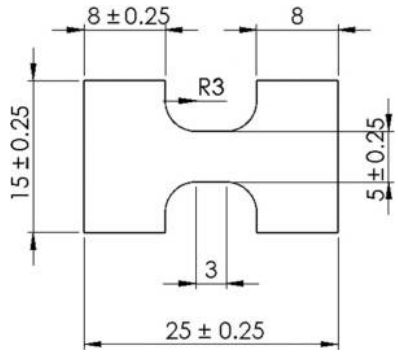

ABS filament to prevent slippage and necking within the jaws. A clamping pressure of 30 psi was found to prevent slip while minimizing filament breakage within the jaws. The metal clamps caused nearly half of the filaments to break within the jaws, so all these data points were discarded, but the results of the remaining specimens were very repeatable. The average strength from six specimens is shown in Figure 5.

Results and discussion

Fiber width and bond width

The measured fiber widths and bond widths are shown in Table II. The bond widths were consistently smaller than the fiber widths, indicating that the adjacent layers never achieved complete wetting. This concept is clearly illustrated by the $f_{wetting}$ column in Table II in which $f_{wetting}$ is defined as the ratio of the bond width to the fiber width. The $f_{wetting}$ factor is expected to greatly influence bond strength because wetting contributes to bond strength and determines the cross-sectional area over which the chains can diffuse (Wool and O'Connor, 1981, 1982).

Stress–strain curves

The stress–strain plot for a typical ABS filament specimen is compared to that of a typical longitudinal part and to a typical bond strength part in Figure 4. The longitudinal specimen approached the yield strength of the constitutive filament, but the longitudinal part had a much smaller elongation at break.

Table I List of the 11 FDM processing conditions

Condition no.	Condition name	Platform temperature (°C)	Nozzle temperature (°C)	Print speed (mm/min)	Fiber width (mm)	Layer height (mm)
1	Reference	125	255	2,000	0.6	0.3
2	Platform 100	100	255	2,000	0.6	0.3
3	Platform 150	150	255	2,000	0.6	0.3
4	Nozzle 230	125	230	2,000	0.6	0.3
5	Nozzle 280	125	280	2,000	0.6	0.3
6	Speed 4,000	125	255	4,000	0.6	0.3
7	Speed 1,000	125	255	1,000	0.6	0.3
8	Width 0.4	125	255	2,000	0.4	0.3
9	Width 0.8	125	255	2,000	0.8	0.3
10	Height 0.45	125	255	2,000	0.6	0.45
11	Height 0.15	125	255	2,000	0.6	0.15

Table II Measured fiber widths and bond widths; $f_{wetting}$ = *Bond width/Fiber width*

Condition no.	Condition name	Fiber width set in software (mm)	Measured fiber width (mm)	Measured bond width (mm)	$f_{wetting}$
1	Reference	0.6	0.69	0.54	0.78
2	Platform 100	0.6	0.66	0.51	0.77
3	Platform 150	0.6	0.69	0.53	0.77
4	Nozzle 230	0.6	0.68	0.51	0.75
5	Nozzle 280	0.6	0.69	0.53	0.77
6	Speed 4,000	0.6	0.59	0.44	0.75
7	Speed 1,000	0.6	0.68	0.49	0.72
8	Width 0.4	0.4	0.45	0.30	0.67
9	Width 0.8	0.8	0.86	0.67	0.78
10	Height 0.45	0.6	0.67	0.40	0.60
11	Height 0.15	0.6	0.67	0.59	0.88

Figure 4 Stress–strain curves showing typical filament, longitudinal and bond strengths

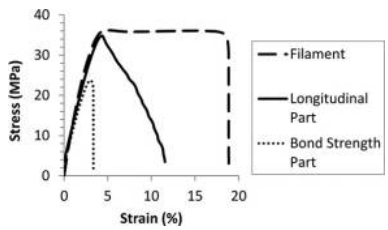

After yielding, the longitudinal fibers began breaking one by one as can be seen by the step changes in the stress profile, resulting in a lower final elongation. Unlike the filament and longitudinal parts, all transverse specimens failed abruptly at the layer interface with a critical stress governed by the bond strength. As expected, the bond strength was much weaker than the longitudinal strength.

Longitudinal strength

The individual values for all the longitudinal strengths are presented in Figure 5. Longitudinal strength did not significantly change because of different processing conditions. The average longitudinal strength was 34.5 MPa, compared to the ideal strength of 36.3 MPa for the filament. The longitudinal strength was slightly weaker than the filament because of the incomplete cross-section of the longitudinal parts: the measured fiber width was used as the thickness, but the thickness at the bonds was smaller than the fiber width as shown in Figure 1, indicating that some of the calculated cross-sectional area was filled with air. If a multi-fiber part was being printed, the adjacent fibers would press into one another, maximizing the area of the printed polymer. However, voids typically exist in FDM parts, resulting in lower strengths than the virgin material (Ahn *et al.*, 2002; Bellini and Güçeri, 2003).

Figure 5 Individual value plot for longitudinal strength

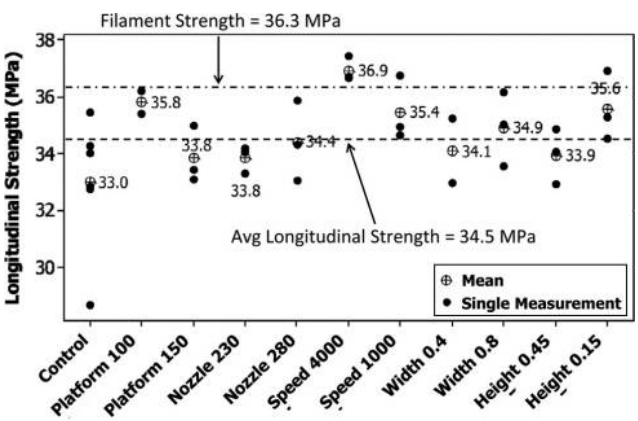

Note: Refer to (Table I) for the processing conditions used for each part

Filament and fiber deviations

A filament of 1 m length was measured to characterize the cross-sectional variations with the results shown in Figure 6(a). The cross-sectional area of the filament varies because of the cyclic pressure fluctuations caused by the screw beat in extrusion (Gaspar-Cunha and Covas, 2014). The filaments are intended to have a 1.75 mm diameter, which would result in a cross-sectional area of 2.40 mm^2. The average cross-sectional area was 2.19 mm^2, which is 8.8 per cent less than the specification. Small filament cross-sections result in smaller fiber cross-sections than intended, which should result in weaker parts. It is interesting to consider that the fiber widths already exceeded the set widths (Table II), and would have been even wider had the filament diameter actually been 1.75 mm, though the fiber width is adjustable by controlling the filament feed rate relative to the print speed and layer thickness.

The variations in filament cross-section were found to propagate directly to variations in the printed fiber cross-section. This result is shown in Figure 6(b) by comparing the deviations from the average fiber area to the average bond strength for the reference condition. The fiber areas were calculated from the fiber widths and heights measured for every layer of a single reference condition part. The bond strength deviations closely follow the variation in the deposited fiber area deviations.

Bond strength

Effect of wall location on strength

Bond strengths were analyzed as a function of the wall from which the specimen was cut. The walls were labeled A to D as shown in Figure 2. Bond strength as a function of the wall location is shown in Figure 7(a) for the reference condition.

Figure 6 (a) Cross-sectional area of the filament (◆) relative to the ideal filament cross-section (–) and (b) deviations in bond strength (◆) compared to deviations in the fiber area (-)

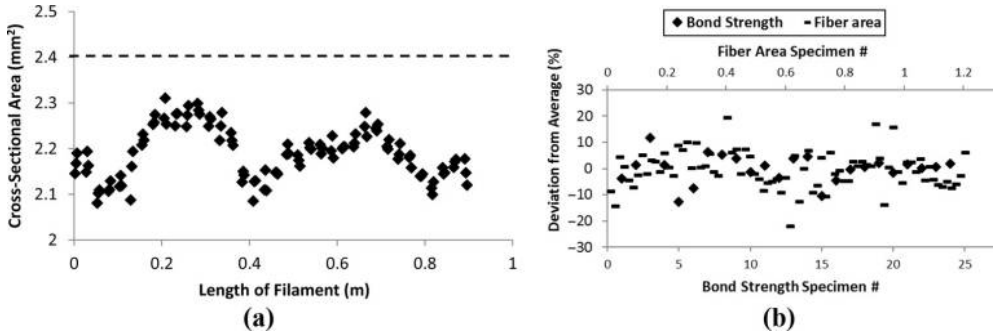

Figure 7 Results as a function of wall side

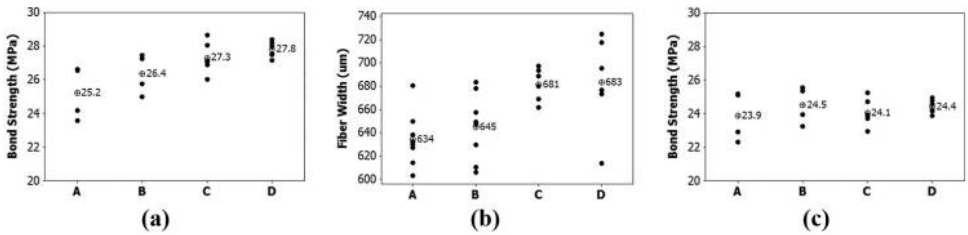

Notes: (a) Bond strength; (b) measured fiber width; (c) and bond strength corrected for the measured fiber widths

There is a clear trend, showing that as the location moves further away from the start of the layer (moves toward wall D), the strength increases. The fiber widths were measured for multiple layers across a single part, and the results are shown in Figure 7(b). As the nozzle moves away from the start of the layer, it extrudes more material, resulting in larger fiber widths. If the average fiber widths for each wall are used to calculate the bond strength for that same corresponding wall, the bond strengths shown Figure 7(c) are calculated. The wall dependence disappears, indicating that the increase in extruded material caused the apparent increase in bond strength as a function of the wall location.

The reason for the fiber width variation of Figure 7(b) is that after the nozzle starts printing a new layer, the extrudate flow rate increases until it eventually reaches equilibrium. To maintain equilibrium, switching layers (or stopping and starting the FDM extruder) should be minimized when designing an FDM part. This partially explains what has been reported in the literature (Singamneni *et al.*, 2012) where parts made through curved layer deposition were stronger because they were made with more continuous layers.

Break height

The location at which all the specimens broke was recorded from 0 (closest to the build platform) to 100 per cent (furthest from the platform) as depicted in Figure 8(a). The break height distribution is shown in Figure 8(b). Specimens broke much more frequently at the top of the specimen because the environment temperature was cooler further away from the build platform as verified with infrared imaging. This finding suggests that diffusion-based healing is the major mechanism driving the bond strength, meaning that higher interface temperatures will result in greater bond strengths. The break height results strongly support this theory, because layers close to the platform had higher interface temperatures and stronger bonds.

Bond strength regression

The bond strength results versus the five conditions are shown in Figure 9. Bond strengths ranged from 40 to 85 per cent of the filament strength, depending on the processing conditions. The multiple regression model of equation (1) describes the bond strength as a function of wall location (*wall*), platform temperature (T_P [°C]), nozzle temperature (T_N [°C]), speed (S [mm/min]), fiber width (W [mm]) and layer height (H [mm]) for the values indicated in Table I. This equation fit well with a coefficient of determination, R^2, equal to 0.904. Smaller heights, larger widths, higher speeds, higher nozzle temperatures and higher platform temperatures all resulted in greater bond strengths. The influence of each condition is described in greater detail in the following sections.

$$Bond = 4.09 + 1.01 \cdot Wall + 0.0515 \cdot T_P + 0.125 \cdot T_N + 0.0013 \cdot S + 26.5 \cdot W - 34.6 \cdot H \quad (1)$$

Influence of platform temperature on bond strength

Platform temperature was the only condition that did not have a statistically significant effect on bond strength. Nonetheless, as shown in Figure 9, there appears to be a trend indicating stronger bonds at higher platform temperatures. Based on the healing model, higher platform temperatures would be expected to create stronger bonds because of a higher interface temperature. However, the break location always occurred over 12 mm away from the build platform, so the platform temperature only had a slight effect on the substrate

Figure 8 Break height (a) analysis and (b) results

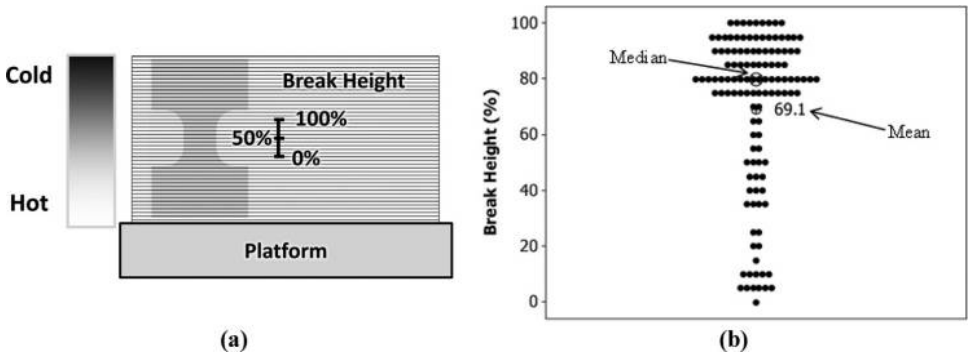

Figure 9 Main effects box plots for bond strength

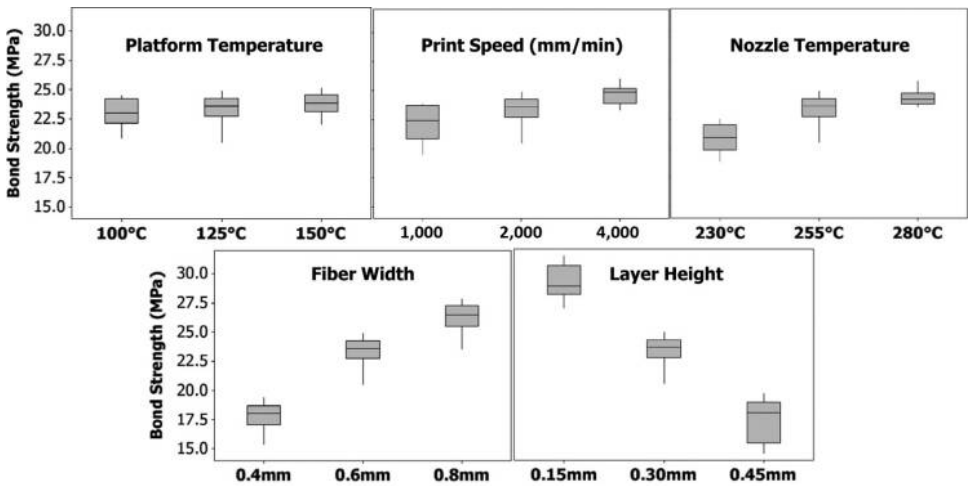

Note: Refer to (Table I) for the processing conditions used for each part

temperature as observed with an infrared camera. The use of a temperature-controlled environment (as opposed to just a temperature-controlled build plate) should provide greater control of bond strength.

Influence of nozzle temperature on bond strength

The nozzle temperature had a significant effect on bond strength because it governs the initial temperature of the fiber being deposited (Dinwiddie *et al.*, 2014). The nozzle temperature, therefore, has a direct effect on the temperature of the interface, which governs the reptation of the polymer molecules and thus the diffusion and healing across the polymer layers. It is, therefore, suggested to process at the highest possible nozzle temperature without degrading the material.

The upper temperature limit for an FDM nozzle prior to degradation may be higher than the supplier recommendation. For instance, Sabic recommends a melt temperature between 220°C and 260°C when injection molding Cycolac MG47. For FDM, however, nozzle temperatures up to 280°C were found beneficial. Degradation is not only temperature dependent but also time dependent, so the residence time of the process is very important. The residence time for FDM at the reference condition for a liquefier length of 20 mm is only 9 s, whereas the residence time in injection molding is often several minutes. It is likely that temperatures even higher than 280°C could be used to maximize part strength during FDM printing of Cycolac MG47; filament produced from polylactic acid is similarly printed at temperatures well above the recommended conditions (Pan *et al.*, 2016).

Influence of deposition speed on bond strength

Faster print speeds resulted in stronger parts as indicated by Figure 9. Literature has also shown similar trends in interlayer strength as a function of print speed (Pan *et al.*, 2016). The likely reason is that each layer has less time to cool before the next layer is deposited, resulting in a higher initial interface temperature and more diffusion. Printing at fast speeds is not only beneficial for bond strength but also improves processing efficiency.

Interestingly, printing at the fastest speed of 4,000 mm/min was the only condition that resulted in thinner fiber widths than specified, as shown in Table II. Fiber widths of 0.60 mm were specified, but the 4,000 mm/min condition produced an average fiber width of only 0.59 mm; the reference, for example, had an average fiber width of 0.69 mm. Producing small fiber widths would be a serious problem when printing full parts because the small fibers would not overlap with one another, creating many voids and minimizing the contact and bond strength between adjacent fibers. Less material may have

been extruded at 4,000 mm/min because the motor did not have enough torque to push out the viscous polymer at 4,000 mm/min. This motor torque limitation could be solved by processing at higher nozzle temperatures or by introducing more powerful feed motors.

Influence of fiber width on bond strength

Other than layer height, fiber width had the largest effect on the bond strength (Figure 9). Fibers with larger widths have more thermal mass, causing them to cool much more slowly; cooling time scales proportionally with thickness squared or radius squared (Malloy, 1994). Larger fibers have been reported to remain above T_g for longer times (Thomas and Rodriguez, 2000; Rodríguez-Matas, 1999; Dinwiddie *et al.*, 2014), meaning more polymer chain diffusion occurs. Larger fiber widths also resulted in more wetting (Table II), which improves bond strength (Li *et al.*, 2002a; Bellehumeur *et al.*, 2004; Wool and O'Connor, 1981, 1982). The longer aspect ratios from larger fiber widths created larger contact areas between layers, increasing the wetted area. It would be best for the bond strength to make the widths as large as possible, but larger widths will limit part resolution.

Influence of layer height on bond strength

Of the conditions studied, layer height had the largest influence on bond strength. Smaller heights resulted in much stronger bonds because they had much higher wetting functions, $f_{wetting}$, as shown in Figure 10 and quantified in Table II. The longer aspect ratios from small layer heights resulted in more contact area between fibers and more wetting. Some specimens from the "Height 0.15" condition had bond strengths above 30 MPa, which was close to the maximum strength of 36.3 MPa for the Cycolac MG47 ABS filament.

The specimens produced at a height of 0.15 mm were on average 70 per cent stronger than those with a height of 0.45 mm, but the bond width was only 47 per cent larger. Therefore, some effect in addition to increased wetting was contributing to the increased strength in parts made with smaller layer heights. Thermally induced chain diffusion was not this additional mechanism: if the layer height affected the cooling of the fibers, the larger heights of 0.45 mm would cool more slowly and therefore have more diffusion.

The increased strength in thin layers could possibly be explained by the increased pressure in the molten fiber during deposition (Table III). The pressure was calculated assuming a rectangular flow channel (the asymmetric shape of the fibers makes this a better assumption than that of a cylindrical flow channel) as shown in equation (2) (Malloy, 1994):

Figure 10 Cross-sectional areas for the fibers produced at the three layer heights

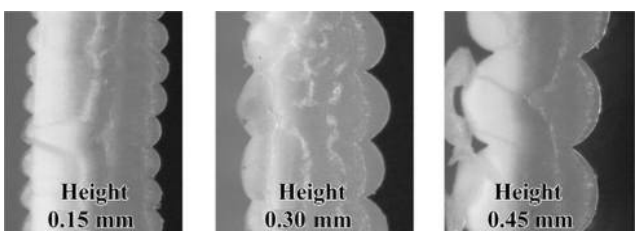

Table III Measured viscosity and calculated flow rate, shear rate and pressure

Condition name	Volumetric flow rate (mm^3/s)	Shear rate (s^{-1})	Viscosity (Pa × s)	Pressure (MPa)
Reference	6	490	350	0.77
Platform 100	6	490	350	0.77
Platform 150	6	490	350	0.77
Nozzle 230	6	490	510	1.1
Nozzle 280	6	490	200	0.44
Speed 1,000	3	240	500	0.55
Speed 4,000	12	980	240	1.0
Width 0.8	8	650	290	0.65
Width 0.4	4	330	430	0.95
Height 0.15	3	240	500	4.4
Height 0.45	9	730	270	0.27

$$\Delta P = \frac{12 \cdot Q \cdot \eta \cdot L}{W \cdot H^3} \tag{2}$$

where L is the flow length in the nozzle, which was assumed to be 0.5 mm, W is the fiber width and H is the layer height. Q is the volumetric flow rate, which was calculated as the layer volume ($W \times H \times$ "layer length", which equals 203.2 mm) divided by the time it took to print a single layer. η is the apparent viscosity of the polymer through the nozzle. The apparent viscosity was based on the nozzle temperature and the shear rate, which was calculated based on a cylindrical flow channel as shown in equation (3) (Malloy, 1994):

$$\dot{\gamma} = \frac{4 \cdot Q}{\pi \cdot r^3} \tag{3}$$

where r is the radius of the nozzle (0.25 mm). The viscosity was determined based on rheological frequency sweep data using a parallel plate rheometer.

Thinner layers require higher extrusion pressures, as shown in Table III and Figure 11. Higher pressures are reported to cause faster intimate contact between interfaces (Butler *et al.*, 1998), meaning thin layers may form intimate contact and wet out more quickly, allowing more total time for diffusion. The higher pressures generated from the thin layer heights are believed to force the two layers into better contact, resulting in greater bond strengths.

Figure 11 Effect of layer height on the pressure within the extruded fiber

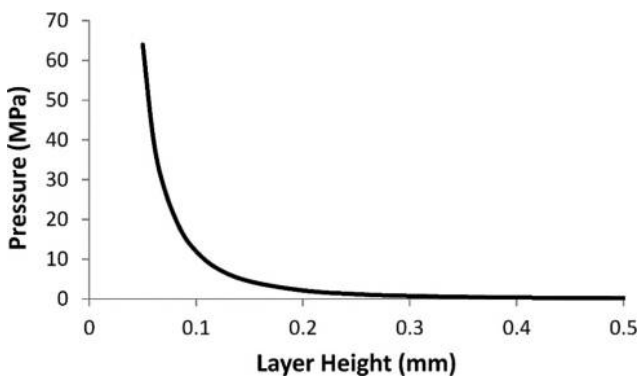

Conclusions

The following process parameters resulted in greater FDM bond strengths: higher platform temperatures, higher nozzle temperatures, faster print speeds, larger fiber widths and smaller layer heights. Smaller layer heights resulted in more wetting and higher pressures exiting the nozzle. The higher pressures are believed to improve the intimate contact between layers. The trends of the other four conditions can be explained by higher interface temperatures resulting in more polymer chain diffusion. This paper recommends using higher nozzle temperatures than those recommended for extrusion and injection molding because of the short residence times during FDM.

Additional findings included the following:

- The vast majority of tensile specimens broke at the cold locations furthest away from the heated build platform.
- Deposited fiber widths increased further away from the start of each layer, indicating that the printer required a certain amount of equilibration time at the start of each layer.
- The variation in filament area correlated to the variation in fiber area and bond strength.
- Less material was deposited at fast print speeds likely because the feed motors did not have enough torque to push out the viscous polymer at those speeds.
- If the fibers are all aligned in the same direction as the tensile test, then bond strength is less of a concern with mechanical properties approaching that of the constitutive filament.

Future work

Higher interface temperatures are believed to cause more polymer diffusion across the interface, based on healing models. The healing model should be confirmed for the non-isothermal FDM process using a heat transfer analysis to model the transient interface temperature. Additionally, the results suggest that pressure and intimate contact play a role in layer-to-layer wetting and, therefore, bond strength. This hypothesis should also be confirmed through modeling and additional experiments. The benefits of processing at higher than expected nozzle temperatures should be explored further by going to nozzle temperatures hotter than 280°C and by performing degradation studies as a function of time and temperature.

References

Ahn, S., Montero, M., Odell, D., Roundy, S. and Wright, P.K. (2002), "Anisotropic material properties of fused deposition modeling ABS", *Rapid Prototyping Journal*, Vol. 8 No. 4, pp. 248-257.

Bellehumeur, C., Li, L., Sun, Q. and Gu, P. (2004), "Modeling of bond formation between polymer filaments in the fused deposition modeling process", *Journal of Manufacturing Processes*, Vol. 6 No. 2, pp. 170-178.

Bellini, A. and Güçeri, S. (2003), "Mechanical characterization of parts fabricated using fused deposition modeling", *Rapid Prototyping Journal*, Vol. 9 No. 4, pp. 252-264.

Butler, C.A., McCullough, R.L., Pitchumani, R. and Gillespie, J.W. (1998), "An analysis of mechanisms governing fusion bonding of thermoplastic composites", *Journal of Thermoplastic Composite Materials*, Vol. 11 No. 4, pp. 338-363.

Dinwiddie, R.B., Kunc, V., Lindal, J.M., Post, B., Smith, R.J., Love, L. and Duty, C.E. (2014), "Infrared imaging of the polymer 3D-printing process", *Thermosense: Thermal Infrared Applications XXXVI Proceedings of the SPIE 9105*, Society of Photo-Optical Instrumentation Engineers, Bellingham, WA.

Espalin, D., Arcaute, K., Rodriguez, D., Medina, F., Posner, M. and Wicker, R. (2010), "Fused deposition modeling of patient-specific polymethylmethacrylate implants", *Rapid Prototyping Journal*, Vol. 16 No. 3, pp. 164-173.

Garg, A., Tai, K. and Savalani, M. (2014), "State-of-the-art in empirical modelling of rapid prototyping processes", *Rapid Prototyping Journal*, Vol. 20 No. 2, pp. 164-178.

Gaspar-Cunha, A. and Covas, J. (2014), "The plasticating sequence in barrier extrusion screws part II: experimental assessment", *Polymer-Plastics Technology and Engineering*, Vol. 53 No. 14, pp. 1456-1466.

Hill, N. and Haghi, M. (2014), "Deposition direction-dependent failure criteria for fused deposition modeling polycarbonate", *Rapid Prototyping Journal*, Vol. 20 No. 3, pp. 221-227.

Li, L., Sun, Q., Bellehumeur, C. and Gu, P. (2001), "Composite modeling and analysis of FDM prototypes for design and fabrication of functionally graded parts", *Solid Freeform Fabrication Symposium, Austin, TX*, Laboratory for Freeform Fabrication and University of Texas at Austin, Austin TX, pp. 1-8.

Li, L., Sun, Q., Bellehumeur, C. and Gu, P. (2002), "Composite modeling and analysis for fabrication of FDM prototypes with locally controlled properties", *Journal of Manufacturing Processes*, Vol. 4 No. 2, pp. 129-141.

Li, L., Sun, Q., Bellehumeur, C. and Gu, P. (2002), "Investigation of bond formation in FDM process", *Solid Freeform Fabrication Symposium, Austin, TX*, Laboratory for Freeform Fabrication and University of Texas at Austin, Austin TX, pp. 1-8.

Malloy, R.A. (1994), *Plastic Part Design for Injection Molding*, Hanser Gardner Publications, Cincinnati, OH.

Pan, A., Huang, Z., Guo, R. and Liu, J. (2016), "Effect of FDM process on adhesive strength of Polylactic Acid (PLA) filament", *Key Engineering Materials*, Vol. 667.

Rodríguez-Matas, J.F. (1999), "Modeling the mechanical behavior of fused deposition acrylonitrile-butadiene styrene polymer components", PhD thesis, Department of Mechanical and Aerospace Engineering, University of Notre Dame, Notre Dame, IN.

Singamneni, S., Roychoudhury, A., Diegel, O. and Huang, B. (2012), "Modeling and evaluation of curved layer fused deposition", *Journal of Materials Processing Technology*, Vol. 212 No. 1, pp. 27-35.

Sun, Q., Rizvi, G.M., Bellehumeur, C.T. and Gu, P. (2008), "Effect of processing conditions on the bonding quality of FDM polymer filaments", *Rapid Prototyping Journal*, Vol. 14 No. 2, pp. 72-80.

Thomas, J.P. and Rodriguez, J.F. (2000), "Modeling the fracture strength between fused-deposition extruded rods", *Solid Freeform Fabrication Symposium*, Austin, TX, pp. 16-23.

Turner, B.N., Strong, R. and Gold, S.A. (2014), "A review of melt extrusion additive manufacturing processes: I: process design and modeling", *Rapid Prototyping Journal*, Vol. 20 No. 3, pp. 192-204.

Wool, R.P. and O'Connor, K.M. (1981), "A theory crack healing in polymers", *Journal of Applied Physics*, Vol. 52 No. 10, pp. 5953-5963.

Wool, R.P. and O'Connor, K.M. (1982), "Time dependence of crack healing", *Journal of Polymer Science: Polymer Letters Edition*, Vol. 20 No. 1, pp. 7-16.

Corresponding author

Timothy J. Coogan can be contacted at: Timothy.J.Coogan@saint-gobain.com